Chemical Deposition of Cu_2O Nanocrystals with Precise Morphology Control

Mariano D. Susman,[†] Yishay Feldman,[‡] Alexander Vaskevich,[†,*] and Israel Rubinstein[†,*]

[†]Department of Materials and Interfaces, Weizmann Institute of Science, Rehovot 76100, Israel, and [‡]Department of Chemical Research Support, Weizmann Institute of Science, Rehovot 76100, Israel

ABSTRACT Copper(I) oxide nanoparticles (NPs) are emerging as a technologically important material, with applications ranging from antibacterial and fungicidal agents to photocatalysis. It is well established that the activity of Cu_2O NPs is dependent on their crystalline morphology. Here we describe direct preparation of Cu_2O nanocrystals (NCs) on various substrates by chemical deposition (CD), without the need of additives, achieving precise control over the NC morphology. The substrates are preactivated by gold seeding and treated with deposition solutions comprising copper sulfate, formaldehyde, NaOH, and citrate as a complexant. Production of NC deposits ranging from complete cubes to complete octahedra is demonstrated, as well as a full set of intermediate morphologies, *i.e.*, truncated octahedra, cuboctahedra, and truncated cubes. The NC morphology is defined by the NaOH and complexant concentrations in the deposition solution, attributed to competitive adsorption of citrate and hydroxide anions on the Cu_2O {100} and {111} crystal faces and selective stabilization of these faces. A sequential deposition scheme, *i.e.*, Cu_2O deposition on pregrown Cu_2O NCs of a different morphology, is also presented. The full range of morphologies can be produced by controlling the deposition times in the two solutions, promoting the cubic and octahedral crystal habits. Growth rates in the ⟨100⟩ and ⟨111⟩ directions for the two solutions are estimated. The Cu_2O NCs are characterized by SEM, TEM, GI-XRD, and UV–vis spectroscopy. It is concluded that CD furnishes a simple, effective, generally applicable, and scalable route to the synthesis of morphologically controlled Cu_2O NCs on a variety of conductive and nonconductive surfaces.

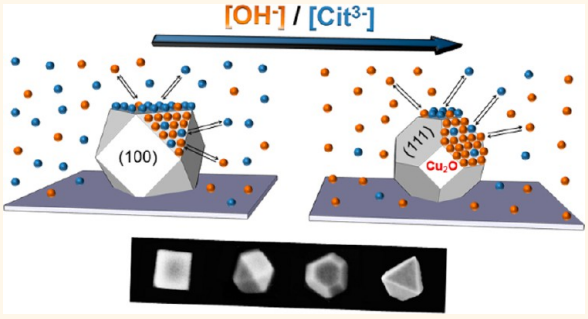

KEYWORDS: cuprous oxide · copper(I) oxide · semiconductor nanocrystals · crystal growth · competitive adsorption · electroless deposition

Controllable preparation of nanostructured metal oxides is an intriguing research area that follows logically the extensive understanding of morphologically controlled face-centered cubic (fcc) metal nanoparticle (NP) synthesis achieved in the last decades.[1,2] Still, due to the more complex compositions of the oxide systems, a high-level understanding of the conditions required for the successful preparation of well-defined metal oxide NPs is rather limited.[3]

Cu_2O is a native p-type semiconductor (bulk direct band-gap energy of 2.17 eV) that is nontoxic and highly abundant in the earth crust. It has a large absorption coefficient over the violet-to-green solar spectrum, making it suitable for conversion of solar to electrical or chemical energy.[4,5] It has been shown recently that n-type Cu_2O can be obtained under special synthetic conditions, which may open the way to more efficient Cu_2O-based solar cells.[4,6] Other applications of interest include Cu_2O as a photocatalyst for solar water splitting[7] and for the degradation of organic pollutants under visible light irradiation[8−11] and in gas sensing.[12,13] It has been used as a catalyst for N-arylation,[14] CO oxidation,[15] and other organic reactions, as well as a negative electrode in Li-ion batteries.[16] Cu_2O colloids have been used as inks in printable conductive interconnects[17] and as antibacterial or antifungal agents,[18] while other properties make them suitable for the preparation of magnetic and superconductive materials, when appropriately doped with metal ions.

* Address correspondence to alexander.vaskevich@weizmann.ac.il, israel.rubinstein@weizmann.ac.il.

Received for review May 22, 2013 and accepted December 29, 2013.

Published online January 08, 2014
10.1021/nn405891g

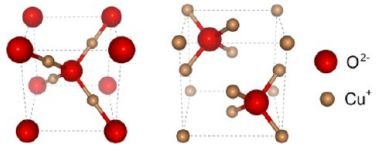

Scheme 1. Possible representations of the Cu_2O crystal lattice structure.

Face-centered cubic Cu_2O is found in nature as cuprite, its crystalline mineral form. The crystal symmetry is cubic (space group $Pn\bar{3}m$), and the structure can be viewed as two interpenetrated sublattices: a body-centered arrangement of O^{2-} anions and an fcc sublattice of Cu^{+} cations (Scheme 1).

A simple and scalable method providing precise and systematic control over the morphology of Cu_2O NPs is highly desirable, as the morphology and size strongly affect the NP electronic structure, physical properties, surface energy, and chemical reactivity.

Chemical (electroless) deposition (CD) of Cu_2O on surfaces represents an easy, scalable, and inexpensive technique for the preparation of nanoparticulate and continuous Cu_2O films on a variety of conductive and nonconductive substrates.

Compared to colloidal synthesis, the use of metastable CD solutions allows convenient separation of the NP nucleation process from the crystal growth, providing an effective tool for understanding the NP growth. In addition, formation of the NPs *in situ* on the substrate surface avoids the need to use additives for stabilizing the colloid, potentially capable of inducing morphological effects. Yet little is known on morphology control in the context of direct CD of Cu_2O NPs on substrates.

CD of Cu_2O continuous films on nonconductive substrates is usually performed by the method of Grozdanov and co-workers;[19,20] however, analysis of the resulting film morphologies and the factors defining their structure has been scarce. Greenberg and Breininger proposed an approach to Cu_2O CD on preactivated glass using HCHO/$CuSO_4$/tartrate/NaOH solutions, typically used for producing metallic Cu.[21,22]

CD of Cu_2O occurs upon immersion of conductive or preactivated substrates in metastable deposition solutions containing $CuSO_4$, NaOH, a reducing agent, and a suitable complexant. In the case of HCHO as the reductant, the following overall chemical reaction is assumed to occur:

$$2CuX^{2-} + HCHO + 5OH^{-} \rightarrow Cu_2O(s) + HCOO^{-} + 3H_2O + 2X^{4-} \quad (1)$$

where X^{4-} is a tetradentate ligand that stabilizes Cu^{2+} in solution at the high pH required for HCHO to exhibit a sufficiently high reducing potential. Typically, EDTA,[23] tartrate,[24] citrate,[25] and NH_3[11] have been employed to avoid the formation of $Cu(OH)_2$ in colloidal and electroless deposition syntheses.

In our study on CD of plasmonic Cu NP films on glass using HCHO and tartrate-based solutions[24] we found that under certain conditions formation of highly crystalline truncated octahedral Cu_2O nanodeposits was attained. While the phase composition was largely defined by the total HCHO and $CuSO_4$ concentrations, the complexant and base concentrations were left unchanged. We hypothesized that, by varying the concentrations of the latter two components, morphological control over the deposited Cu_2O nanocrystals (NCs) could be achieved. This hypothesis was strengthened by analyzing a variety of chemical conditions typically used in colloidal Cu_2O syntheses[9,26] and in electrodeposition of Cu_2O particles on conducting substrates.[27−29]

Various groups have studied the formation of Cu_2O colloids.[30,8−11,14,26] Preparations include hydrothermal,[23,31,32] polyol,[33] sonochemical,[34] and direct chemical syntheses,[9,11,26,30,35−39] using ascorbic acid,[26,30,36] sodium ascorbate,[8,14,35] hydrazine,[11,14] or hydroxylamine[9,10] as reducing agents. Numerous chemical syntheses of Cu_2O colloids have made use of a variety of surfactants and capping agents, such as SDS,[8−10,29] PVP,[26] CTAB,[35] and PEG,[36] to stabilize and/or direct the morphology of the colloid. The inclusion of such additives introduces additional complexity compared to CD or electrochemical deposition, due to possible adsorption and stabilization of particular facets exerted by the additive. Several authors have pointed out the possibility of controlling the Cu_2O colloid morphology without using surfactants or other colloid stabilizers. Morphological control was claimed to be achieved by controlling the concentration ratios [reducing agent]/[Cu^{2+}], [OH^{-}]/[Cu^{2+}], and [complexant]/[Cu^{2+}] and/or by changing the reducing agent.[11,14,30,40,41] However, since changes in [reducing agent] and [Cu^{2+}] concentrations during CD could lead to metal deposition,[24] varying the [complexant] and [OH^{-}] appears more suitable for achieving shape control in CD of Cu_2O.

In many colloidal syntheses, increasing the alkalinity during preparation with minimal variation of the other solution components has led to an increase in particle size, with little variation of the morphology.[9,11,30] The effect of the alkali concentration on the NP morphology in Cu_2O colloidal synthesis has remained largely unclear.[41]

With respect to complexants, stabilization by preferential adsorption of aminated complexants on Cu_2O {111} faces during crystal growth was reported for NH_3 and EDTA.[11,23] A similar behavior was observed with aminated reducing agents, such as hydrazine or hydroxylamine.[10] We are not aware of any complexant or reductant proven conclusively to stabilize Cu_2O{100} facets.

Extensive studies of Cu_2O NC morphology have been carried out in the context of electrodeposition

on conductive substrates, forming either continuous or isolated NP films.[42,43] Varghese and co-workers[44−46] have laid the foundation for electrodeposition of continuous Cu_2O thin films;[44−46] however, crystal habits were not controlled. Switzer and co-workers[47,48] produced continuous Cu_2O films on stainless steel cathodes from alkaline $CuSO_4$−lactate solutions in the potentiostatic mode. The film texture was controlled by fixing the pH; at pH = 12 films displaying a (111) texture were obtained, while at pH = 9 films showing a (100) texture were formed, indicating a strong interaction between OH^- and Cu_2O {111} faces. Choi and co-workers[27−29] performed cathodic galvanostatic Cu_2O deposition on polycrystalline Au electrodes; morphology control was achieved by pH-dependent preferential adsorption of SDS on the {111} faces.

Deposition of Cu_2O thin films was also reported using activated reactive evaporation,[49] pulsed laser deposition,[50] thermal evaporation,[51,52] reactive radio frequency magnetron sputtering,[53] molecular beam epitaxy,[54] thermal[55,56] and anodic oxidation of bulk Cu,[57] and a sol−gel-like dip technique.[58] However, morphological control was hardly achievable in these cases.

In the present work, a method allowing precise control over the morphology of Cu_2O NC deposit prepared by a straightforward CD procedure is introduced for the first time. The deposition is carried out at room temperature on Au-seeded glass substrates, without any special additives. We show that the relative surface energies of the crystal faces are affected by the solution composition, *i.e.*, the NaOH and the sodium citrate (Na_3Cit) complexant concentrations. While hydroxide anions selectively stabilize the Cu_2O {111} facets, citrate ions preferentially stabilize the {100} facets. The competitive adsorption of these ions on the different crystal faces enables precise control over the Cu_2O NC morphology in the entire range from octahedral to cubic.

It is also shown that solutions producing cubic or octahedral crystal habits can be used to shift the morphology of pregrown crystals, such that the final morphology can be designed by choosing appropriate exposure times to each of these solutions. By analyzing the size and shape changes during single-step and two-step depositions, the crystal growth rates in the ⟨100⟩ and ⟨111⟩ directions are estimated.

RESULTS AND DISCUSSION

We have previously shown that deposition solutions comprising 0.177 M sodium potassium tartrate (NaKT), 0.5 M NaOH, 80 mM $CuSO_4$, and 40 mM HCHO produce nanostructured deposits on Au-seeded glass slides, which, up to 20 min deposition, are mainly composed of truncated octahedral Cu_2O NCs.[24] Increase of the NaKT concentration in the deposition solution showed a tendency of shifting the Cu_2O NC morphology to more cubic-like.[59] However, high NaKT concentrations led to co-deposition of metallic copper, especially at longer times,[24] thus precluding deposition of pure cubic Cu_2O deposits. Therefore, new solution compositions were sought for the preparation of Cu_2O NCs with precise morphological control over a full range of morphologies.

Sodium citrate (Na_3Cit) has been used in combination with other reducing sugars or hydroxo-carboxylic acids, such as ascorbic acid or glucose, to obtain Cu_2O (as in the Benedict reagent),[39,41] and in particular for the preparation of cubic-like Cu_2O colloids, in the absence of surfactants and nitrogenated molecules, which stabilize the {111} crystal planes.[60] Consideration of our results with NaKT-based solutions[24] and analysis of previously published works have led us to the hypothesis that hydroxo-carboxylic acids stabilize the Cu_2O {100} facets.[35] As there are no known metastable CD solutions containing ascorbic acid or glucose as reducing agents for producing Cu or Cu_2O, we replaced the complexant with the hydroxo-carboxylic acid citrate (Na_3Cit), with the aim of obtaining the full range of possible Cu_2O NC morphologies while avoiding the formation of metallic Cu.

Activation of the glass substrate by Au seeding is required for Cu_2O deposition to proceed. This is achieved by silanization with 3-aminopropyl trimethoxysilane (APTS) followed by formation of small Au clusters (see Experimental Section), to produce a catalytic layer suitable for facilitating Cu_2O deposition[24,61] (Scheme 2a).

All the Cu_2O depositions described herein make use of 8 mM HCHO in solution, ensuring mild reducing conditions,[24] and a 10-fold Cu^{2+} concentration (80 mM), implying the absence of Cu^{2+} mass-transport limitations under all tested conditions. For controlling the Cu_2O NC morphology, a range of Na_3Cit and NaOH concentrations were explored. A representative set of CD solutions, labeled A to G, is presented in Scheme 2b.

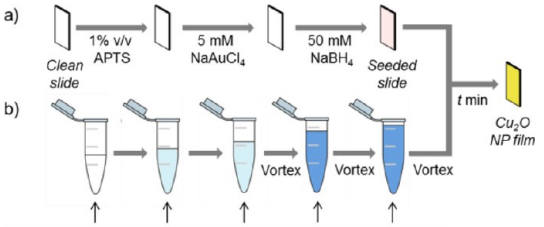

Sample	1.5 M Na_3Cit (S1)	0.64 M $CuSO_4$ (S2)	H_2O	5 M NaOH (S3)	0.32 M HCHO (S4)
A	0.67	0.25	0.83	0.20	0.05
B	1.07	0.25	0.43	0.20	0.05
C	1.20	0.25	0.30	0.20	0.05
D	1.35	0.25	0.15	0.20	0.05
E	1.35	0.25	0.20	0.15	0.05
F	1.35	0.25	0.25	0.10	0.05
G	1.60	0.25	0	0.10	0.05

Scheme 2. (a) Activation of glass substrates by Au seeding. (b) Preparation of deposition solutions. Immersion of a seeded substrate (a) in a deposition solution (b) for *t* min produces Cu_2O NCs with a well-defined crystalline morphology. (Volumes in the table are in mL.)

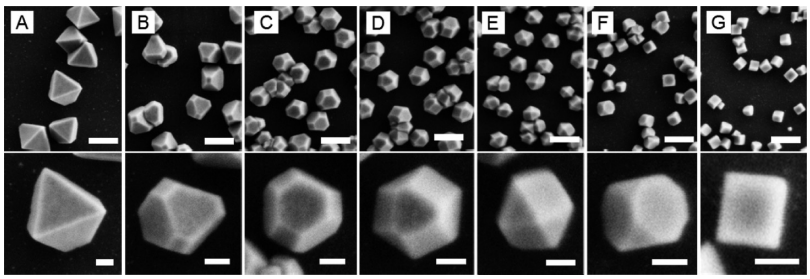

Figure 1. HRSEM images of CD Cu_2O NCs on glass substrates, prepared as in Scheme 2 (using citrate as the complexant and 10 min deposition). Crystal morphology: (A) complete octahedra, (B) tip-truncated octahedra, (C) truncated octahedra, (D) truncated octahedra, (E) cuboctahedra, (F) tip-truncated cubes, and (G) complete cubes. Scale bars: 200 nm (top), 50 nm (bottom).

After immersing activated substrates for 10 min in the CD solutions, followed by rinsing and drying, NCs were observed by HRSEM (Figure 1). Sample A consists of complete octahedral crystals exposing {111} planes only. Increase the citrate concentration (from sample A to D) leads to formation of crystals exposing increasingly large {100} facets. By decreasing the NaOH concentration in the solution (from sample D to F), a similar trend is found, and tip-truncated cubes are obtained. Further increase in [Na_3Cit] results in complete cubes, exposing {100} planes only (sample G).

In our system, by adding the reagents in the order shown, no observable colloid is formed at any stage of the CD (no turbidity is observed when shining a green laser beam through the tube). In several reported Cu_2O colloidal syntheses Cu_2O nucleation in solution was observed, followed by aggregation/Ostwald ripening and surface restructuring to give the final crystalline product after a certain aging period.[8,9] When the restructuring is not complete, the texture of the exposed planes remains rough, evidently constituting smaller particles, as observed by high-resolution microscopies. In highly alkaline colloidal syntheses, visible pale blue $Cu(OH)_2$[10,11,14,26,30,36,38] and even dark brown CuO[26,40] often form prior to addition of the reducing agent, considered as the chemical Cu_2O precursors. Their formation depends strongly on the specific reaction conditions used, and their involvement in the Cu_2O formation pathway should be tested in each case. In our system we avoid bulk solution nucleation and restructuring processes. By using Au-seeded glass and freshly prepared CD solutions, Cu_2O NC formation proceeds solely *via* crystal growth on the preformed Au nuclei.[24] Most NC facets appear quite smooth, indicating the absence of secondary nucleation. Note that Cu(II) reduction in the presence of citrate and absence of formaldehyde was not observed, under any conditions.

In our deposition solutions, the major copper species present are copper(II)-hydroxo-citrate complexes.[62] The stability of these complexes was established as follows: When solution A was prepared without NaOH, the Cu(II)-citrate complex absorption band appeared at 740 nm (Figure S1, Supporting Information). According to the spectrochemical series, OH^- may exert a higher ligand field than the carboxylate groups of the complexant, leading to a higher absorption energy. When NaOH was added (thus producing solution A), the absorption peak blue-shifted to 685 nm, indicating the formation of Cu(II)-hydroxo-citrate species. With a large excess of NaOH, the spectral maximum further blue-shifted to 660 nm, implying formation of more hydroxylated species, probably $[Cu(OH)_4]^{2-}$, believed to exist at very high pH.[63] Therefore in our solutions copper(II)-hydroxo-citrate species are likely to be predominant, as increasing [Na_3Cit] and decreasing [NaOH] (*i.e.*, moving from solution A to G) lead to an equilibrium less shifted toward formation of $[Cu(OH)_4]^{2-}$.

The effect of varying the reagent concentration can be evaluated by considering eq 1 as the sum of two half-reactions, eqs 2 and 3 (disregarding the exact Cu(II) speciation):

$$2CuX^{2-} + 2OH^- + 2e^- \rightarrow Cu_2O(s) + H_2O + 2X^{4-} \quad (2)$$

$$HCHO + 3OH^- \rightarrow HCOO^- + 2H_2O + 2e^- \quad (3)$$

While the copper reduction potential (E_{Cu}) is shifted negatively as [Na_3Cit] is increased, the HCHO oxidation potential (E_{HCHO}) is essentially unaffected.

The net shift in the reduction potential due to increase in the complexant content and stabilization of the Cu(II) species in solution is seen, for samples A to D, as a decreasing net growth rate of the individual NCs, seen as decreasing NC major axis lengths (Table 1 and Figure S2, Supporting Information), from 197 to 135 nm. In parallel, a higher activity of the Au seeds acting as nucleation centers for Cu_2O deposition is observed, increasing the NC surface density from 7.0×10^8 to 3.1×10^9 cm^{-2}; this effect is yet to be understood.

There is a maximal usable [Na_3Cit], dictated by the Na_3Cit solubility limit, slightly higher than 1.5 M. The lower limit of usable Na_3Cit is given by the $Cu(OH)_2$ solubility. When [Na_3Cit] was decreased to 0.24 M,

TABLE 1. HRSEM Image Analysis of Cu_2O NCs as in Figure 1,[a]

		NC dimensions						
sample	morphology	major axis (nm)	*a* (nm)	*b* (nm)	*c* (nm)	*d* (nm)	*R*	NC surface density (cm^{-2})
A	octahedra	197 ± 24			186 ± 21	NM	≥1.732	7.0×10^8
B	tip truncated octahedra	160 ± 29			84 ± 8	35 ± 3	1.34 ± 0.01	1.8×10^9
C	truncated octahedra	157 ± 26			52 ± 4	48 ± 4	1.17 ± 0.01	2.9×10^9
D	truncated octahedra	135 ± 24			29 ± 4	58 ± 6	1.04 ± 0.01	3.1×10^9
E	cuboctahedra	115 ± 16	NM	62 ± 5	NM	62 ± 5	0.866	3.8×10^9
F	tip truncated cubes	97 ± 19	28 ± 3	30 ± 3			0.721 ± 0.008	3.2×10^9
G	cubes	73 ± 14	55 ± 9	NM			≤0.577	4.8×10^9

[a] Errors indicate standard deviations. *R* ratios were calculated for individual particles and averaged. NM = not measurable.

incomplete solubilization of Cu^{2+} was evident by the formation of $Cu(OH)_2$ (a light blue solid). Under these conditions octahedral Cu_2O NCs were produced together with fibrous-like particles, also growing on the Au seeds (Figure S3, Supporting Information). The latter are believed to be CuO nanoleaves together with $Cu(OH)_2$ fiber bundles. Cu_2O deposition under very low [Na_3Cit] was therefore avoided.

In samples D to F, where [NaOH] is decreased, the NC surface density remains approximately constant, whereas the NC size decreases at lower pH (Table 1). The latter may be related to the fact that the net reaction (eq 1) is thermodynamically favored at higher pH. A minimal [NaOH] is also required, below which very slow or no deposition is observed. Further increase in [Na_3Cit] (solution G) shows additional increase in the NC surface density. Interconnected Cu_2O particles may result from growth on closely spaced active seeds. Note that the seeding efficiency was not perfectly reproducible; therefore trends in the Cu_2O NC surface density (NCs per unit area) were determined using the same seeding batch.

Etching processes, defined herein as processes leading to removal of material through surface reduction−oxidation reactions, may occur in the present system, which is open to air. Specifically, Cu_2O NCs can be etched by reaction with dissolved oxygen and complexant (eq 4):

$$2Cu_2O(s) + O_2(aq) + 4H_2O + 4X^{4-} \rightarrow 4[CuX]^{2-} + 8OH^- \quad (4)$$

Increase in the [complexant] and decrease in [OH^-] (from solution A to G) would promote higher etching rates. An etching rate comparable to that of the chemical growth would imply a net growth rate in a particular crystalline direction and a crystal habit that depend on the rates of both the CD and etching. Intuitively, the probability of the latter situation occurring seems low, as the nominal [HCHO] in our system is *ca.* 40 times larger than $[O_2]_{sat}$ in water (*ca.* 7 mg/L or ~0.2 mM);[64] hence O_2 reduction by HCHO is likely to occur in the bulk solution such that the actual [O_2] is expected to be negligible.

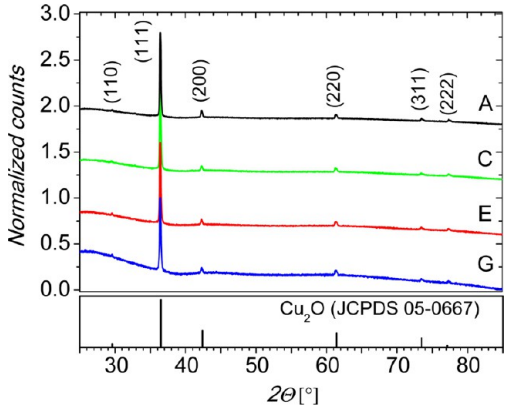

Figure 2. Grazing-incidence XRD (GIXRD) patterns of samples A (octahedra), C (truncated octahedra), E (cuboctahedra), and G (cubes) (Figure 1) on glass substrates. Peaks are assigned to fcc Cu_2O according to JCPDS No. 05-0667 (bottom panel).

To substantiate experimentally the insignificant role of Cu_2O etching in our solutions, supported octahedral Cu_2O NCs were exposed to solution G, in which the $CuSO_4$ fraction was replaced by water to avoid Cu_2O deposition, while maintaining a similar etching ability. After 10 min immersion no morphological change was observed in the NCs (Figure S4, Supporting Information) (some chemical reduction and mass transfer of Cu to the Au seeds is seen). If the octahedral Cu_2O crystals are exposed to solution G, in which the HCHO fraction was replaced by water, minimal etching at crystal edges is observed, likely to be less pronounced in the presence of HCHO. These experimental results rule out the influence of Cu_2O crystal etching on crystal shape under the present deposition conditions.

The phase composition and structure of the deposits were evaluated by grazing-incidence X-ray diffraction (GIXRD). Diffraction patterns of complete octahedra, truncated octahedra, cuboctahedra, and cubes (*i.e.*, samples A, C, E, and G in Figure 1, respectively) are shown in Figure 2. Peaks in the XRD patterns are indexed as the (110), (111), (200), (220), (311), and (222) reflections, corresponding to the cubic-phase crystal structure of cuprite (JCPDS No. 05-0667). The calculated lattice parameter is 4.27 Å, in agreement

with previously reported values.[37,40] No evidence of Cu, CuO, or $Cu(OH)_2$ is found. Due to their much smaller size compared to the Cu_2O NCs, Au seeds are not detected in the diffraction pattern. The relative intensity of the peaks is similar for all the deposits (Figure 2), suggesting that the NCs are randomly oriented with respect to the substrate.[9]

The other intermediate samples are assumed to behave similarly, as supported by the regular (Figure 1) and tilted-angle (Figure S5, Supporting Information) SEM images. It is important to note that the tilted-angle images (Figure S5, Supporting Information) clearly show that the NCs are partially cut on the substrate side, as a result of the asymmetry exerted by the substrate during NC growth.

The phase identification by GIXRD and HRSEM was verified using TEM characterization (Figure 3). Cu_2O NCs were deposited on carbon-coated, Au-seeded TEM grids (prepared as detailed in the Experimental Section). The Au clusters show an average diameter of 2.5 ± 0.1 nm (Figure 3a), producing a diffuse electron diffraction (ED) pattern characteristic of polycrystalline Au (inset in Figure 3a). The Au cluster size determined by

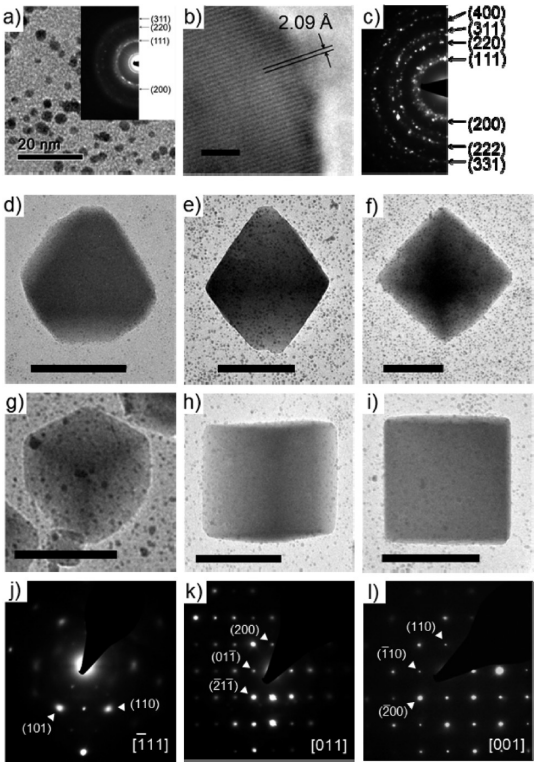

Figure 3. TEM images and ED patterns of CD Cu_2O NCs. (a) Image and ED pattern of Au clusters produced on a carbon-coated, Au-seeded TEM grid. (b) Crystal lattice spacing measured on a Cu_2O NC using high-resolution TEM. (c) ED pattern of an ensemble of Cu_2O NCs; some reflections are assigned. (d–i) TEM images of single NCs prepared using solutions A (d–f) and G (g–i), observed along the (d, g) [111], (e, h) [110], and (f, i) [100] directions; scale bars: (d–f) 100 nm, (g–i) 50 nm. (j-l) Corresponding SAED patterns for octahedral Cu_2O NCs. Zone axes are indicated at the bottom right.

TEM is consistent with Au clusters on activated glass substrates, which are barely seen by SEM, being close to or below the resolution limit of the instrument.[24] The catalytic Au clusters are observed as smaller scattered dots in the background of the Cu_2O NCs' TEM images (Figure 3d–i).

The Cu_2O phase displays a lattice spacing of 2.09 Å, measured under high magnification, corresponding well to the known Cu_2O {200} lattice spacing (Figure 3b).[33,65] The ED pattern of a collection of Cu_2O NCs shows the expected dotted ring pattern, with reflections assigned to the (111), (200), (220), (311), (222), (400), and (331) spacings (Figure 3c).

The TEM images furnish 2D morphological information from the contour angles of the NCs (Steno's law), as well as 3D information from contrast differences in the NC projection, reflecting thickness variations (Figure 3d–i). The results for cubes and octahedra are in agreement with those obtained by HRSEM imaging on glass slides (Figure S6, Supporting Information). Selected-area electron diffraction (SAED) patterns of properly oriented octahedral Cu_2O NCs show typical single-crystal patterns of fcc particles, recorded for selected zone axes (Figure 3j–l). Hence, formation of single-crystalline Cu_2O NCs is confirmed by both imaging and diffraction.

In principle, NC growth cannot proceed under thermodynamic equilibrium conditions; hence the Cu_2O crystals do not necessarily display the most stable crystalline morphology, at least during crystal growth. However, for our discussion we assume that the NCs grow under conditions close enough to equilibrium to justify the use of equilibrium considerations and that the crystal shape is maintained after removing the sample from the solution.

According to the Gibbs–Curie–Wulff theorem, the equilibrium form of a free crystal of a given volume presents the minimal total surface energy (ΔG_s). For a faceted crystal, minimization of $\Delta G_s = \Sigma \gamma_i s_i$ (where γ_i is the specific surface energy per unit area for the *i*-type facet and s_i is the corresponding exposed area) gives the thermodynamically most stable crystal morphology (Wulff's construction). For a crystal at equilibrium, "the distances of the crystal faces from a point within the crystal (called the Wulff's point), h_i, are proportional to the corresponding specific surface energies, $\gamma_i/h_i = constant$" (Scheme 3a).[66] In other words, Wulff's theorem can be stated as "the crystal growth rate perpendicular to any facet is proportional to its surface energy".[26,29] Therefore facets with lower surface energy will tend to dominate over the high-energy facets on the crystal surface.

The equilibrium shape of a crystal deposited on a surface, according to Wulff–Kaishew[66–68] or Winterbottom[69] theorems, will be preserved, although the crystal will be truncated by the substrate, with a truncation that depends upon the crystal–substrate

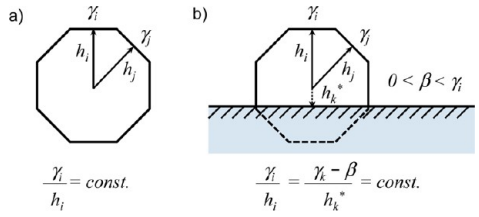

Scheme 3. (a) Wulff and (b) Wulff–Kaishew theorems. The contact face is assumed to be parallel to the crystal plane *i*.

specific adhesion energy (β). The corresponding relationship is $\gamma_i/h_i = (\gamma_k - \beta)/h_k^*$ = constant, where h_k^* is the distance from the Wulff point to the substrate–nanocrystal interface in the direction perpendicular to the *k*th plane (Scheme 3b).

CD of Cu_2O on glass under the present conditions appears to follow the Wulff–Kaishew theorem, with the surface energies of the {100} and {111} crystal planes being dictated by the composition of the deposition solution.

The simplest Wulff–Kaishew model assumes an isotropic β; that is, it neglects possible NC–substrate lattice mismatch during epitaxial growth of differently oriented NCs. This condition is fulfilled in our case as a result of the amorphous nature of the silanized substrates. As the area occupied by the Au seeds is minute compared to the free silanized glass surface, the deposit–substrate interaction (β) is governed by the silane–Cu_2O interaction.

On the basis of the Wulff–Kaishew formulation, crystal shape analysis allows comparison of the relative surface energies of the crystalline facets present on the Cu_2O NCs. The ratio of growth rates perpendicular to the {100} and {111} planes, $R = r_{\langle 100\rangle}/r_{\langle 111\rangle}$, which is proportional to the ratio of surface energies, $\gamma_{100}/\gamma_{111}$, is related to the NC morphology by eqs 5 and 6 (see Supporting Information):[40,70–72]

$$R = \frac{1}{\sqrt{3}}\left(\frac{a+\sqrt{2}b}{a+\frac{2}{3}\sqrt{2}b}\right) \quad \text{for} \quad \frac{1}{\sqrt{3}} \le R \le \frac{1.5}{\sqrt{3}} \qquad (5)$$

$$R = \sqrt{3}\left(\frac{c+d}{c+2d}\right) \quad \text{for} \quad \frac{1.5}{\sqrt{3}} \le R \le \sqrt{3} \qquad (6)$$

For each prepared morphology the edge lengths were measured from HRSEM images, and *R* ratios were calculated (Table 1). *R* values of samples A to G appear to be correlated with the [NaOH]/[Na_3Cit] ratio.

The morphologies of NCs produced in solutions A–G, as well as others obtained under constant [Na_3Cit] or constant [NaOH], are summarized in the morphology diagram presented in Figure 4. It is clear that cubes ($R_G = \gamma_{100}/\gamma_{111} \le 0.577$) are produced when [$Na_3Cit$] is high and [NaOH] is low, while octahedra ($R = \gamma_{100}/\gamma_{111} \ge 1.732$) form when [$Na_3Cit$] is low and [NaOH] is high. While there is a correlation between *R* and the [NaOH]/[Na_3Cit] ratio, the latter is not sufficient

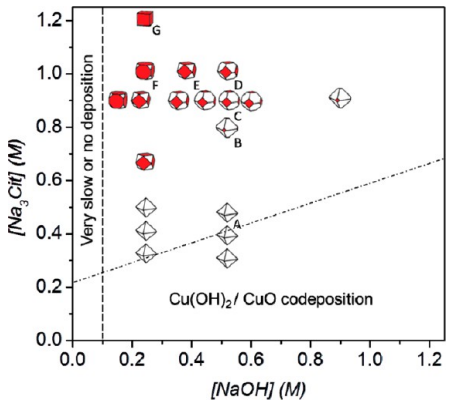

Figure 4. Morphology diagram: Cu_2O morphologies obtained in CD solutions of different NaOH and Na_3Cit concentrations. Samples A–G (Scheme 2, Figure 1, and Table 1) are marked.

for defining the final crystal morphology, which also depends on the absolute concentrations.

When [Na_3Cit] is increased at constant [NaOH], *i.e.*, under conditions where the effect of the citrate anions can be evaluated independently, *R* decreases (Figure 4). This leads to the conclusion that citrate anions preferentially adsorb on the {100} Cu_2O facets, thereby stabilizing these crystal faces and lowering their surface energy.[73] When [NaOH] is increased at a constant [Na_3Cit] (Figure 4), the *R* ratio is increased, favoring octahedral crystal habits. The OH^- anions therefore preferentially adsorb on the {111} Cu_2O facets, thus selectively stabilizing these crystal faces.

Bulky citrate anions might have a favorable cooperative interaction with {100} facets *via* the multiple carboxylate groups, which may not be that effective on {111} faces, possibly due to the different surface ionic arrangement. If the {100} planes are selectively stabilized by citrate, and therefore crystal growth is hindered in the ⟨100⟩ directions, {100} planes would grow slower than {111} planes, and the final morphology would shift to a cube.

Ideal stoichiometric Cu_2O {100} surfaces were modeled to be polar and with a square symmetry.[74] During crystal growth the Cu_2O surface charge alternates between positive (Cu^+-terminated) and negative (O^{2-}-terminated). Positive Cu-terminated facets may be responsible for the interaction with negatively charged citrate ions, resulting in their stabilization during growth. Note that adsorption on and stabilization of polar Cu_2O{100} facets by anions such as Cl^- and NO_3^- were previously reported.[28]

Ideal nonpolar Cu_2O {111} facets contain Cu(I) ions with dangling bonds, which may strongly interact with appropriate species.[10,26,74] The small and high-charge-density OH^- anion can interact with these local dangling bonds, with a higher affinity compared to citrate, Cu(II)-citrate complexes, or methylene glycolate anions, also present in the reaction medium,[41,42] thus stabilizing these crystal faces selectively as compared

to the {100} facets. The morphology would then shift to octahedral. OH^- adsorbed on the {111} surface may also become part of the Cu_2O crystal structure as O^{2-}. The dual role of OH^- ions as a surface-stabilizing agent and participant in NC growth is reasonable assuming that the time scale of the two processes is largely different.

A possible alternative explanation for the observed trends in the NC morphology would involve the assumption that different Cu(II) species present in the deposition solution promote different Cu_2O morphologies. For example, it could be conceived that $[Cu(OH)_4]^{2-}$ favors the octahedral morphology, while the Cu(II)-hydroxo-citrate complexes favor the cubic morphology. However, the lower chemical similarity within the Cu(II)-hydroxo-citrate/OH^- pair makes this pair more likely to exert competitive adsorption rather than different Cu(II) species. Computational simulations (not carried out in the present work) are required to substantiate the latter point.

It is noteworthy that equal deposition times produce octahedral particles (Figure 1A) that are larger than the cubic ones (Figure 1G). The growth rates in solutions A and G can be quantified as the slope of the NC characteristic dimension *vs* time of deposition, giving $r^{A}_{\langle 111\rangle} = 2.6 \pm 0.2$ nm/min and $r^{G}_{\langle 100\rangle} = 1.5 \pm 0.3$ nm/min (Figure 5).

The results in Figure 5, showing preservation of the morphology during single-step NC growth, indicate that the Cu_2O NC morphology is fully defined by the bulk solution composition with no morphological changes occurring during the deposition, at least after a short initial period (<3 min). After acquiring a certain minimal size, the NC growth rate is approximately constant throughout the process. Linear growth of the NC dimension with deposition time implies a constant deposition rate under kinetic (rather than mass transport) control, probably governed by the kinetics of HCHO oxidation (eq 3), in analogy with the mechanism proposed for Cu^0 deposition, where cleavage of the carbon–hydrogen bond of methylene glycolate was the rate-determining step.[75] Note that for all the depositions studied here the estimated bulk solution composition does not change by more than 5% for any of the reagents.

Application of other complexants, such as EDTA and tartrate, was also evaluated, with the former producing morphologically more complex crystals as a result of the existence of {110} facets in the morphologies described above (Figures S7 and S8, Supporting Information). Co-deposition of Cu precludes the use of tartrate and EDTA at high complexant concentration; nevertheless, tartrate showed a similar stabilizing effect toward Cu_2O {100} facets to citrate, supporting our hypothesis of hydroxo-carboxylates stabilizing these facets (Figure S9, Supporting Information). These results indicate that the choice of complexant is crucial for Cu_2O NC shape design.

It is concluded that careful choice of the concentrations of OH^- and citrate anions in the reaction medium allows precise control of the morphology of CD Cu_2O NCs. Competitive adsorption of OH^- and citrate on the {111} and {100} Cu_2O faces alters the relative surface energy of these crystalline facets during growth, enabling convenient tuning of the morphology from complete cubes to complete octahedral *via* intermediate morphologies.

Optical Properties. Extinction spectra of Cu_2O colloids are usually characterized by a series of bands in the UV–vis region, showing large spectral variability for different sample preparations.[9,30,39,76] The latter was attributed to quantum size effects for small enough particles (not relevant to the present study), scattering effects in larger particles, and crystal defects created during synthesis (Cu^+ or O^{2-} vacancies, or other impurities), interparticle distance (interconnection), and more.[39,55,76]

Normalized extinction spectra of the Cu_2O NC films on glass are shown in Figure 6a for samples A–G,

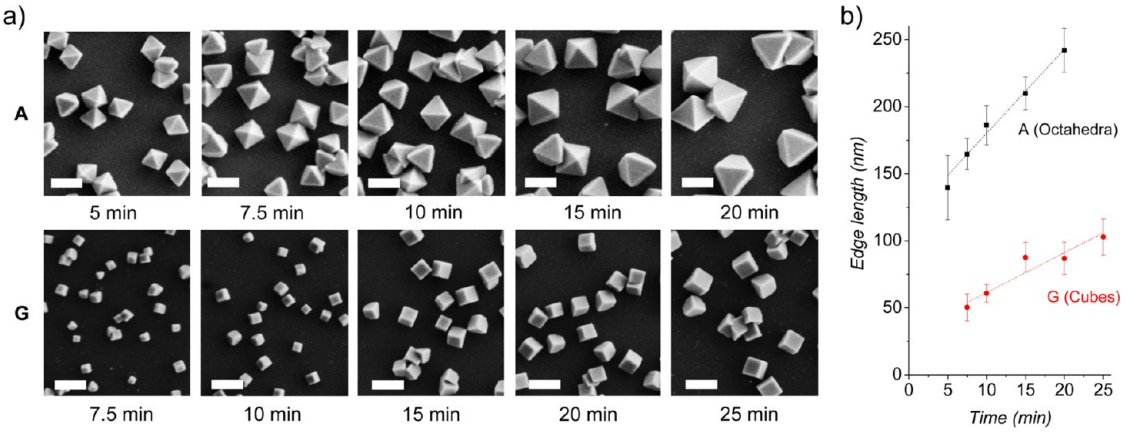

Figure 5. Cu_2O NC size evolution. (a) SEM images of glass slides treated with solutions A and G, forming octahedra and cubes, respectively, for given deposition times (indicated). Scale bars: 200 nm. (b) Characteristic edge lengths as a function of deposition time for these morphologies. Calculated slopes: A, 6.3 ± 0.4 nm/min; G, 3.0 ± 0.5 nm/min.

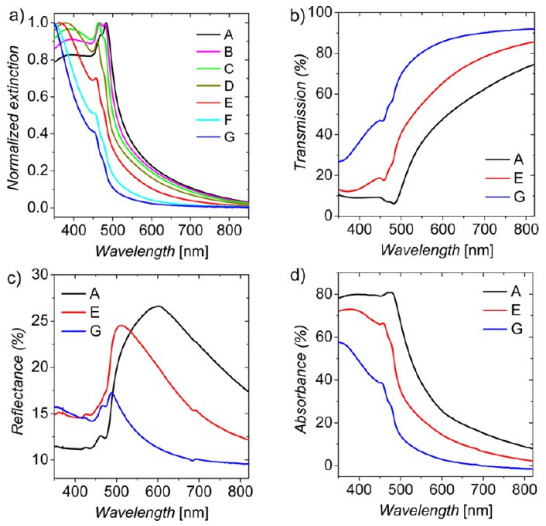

Figure 6. Optical properties of Cu_2O NCs deposited on glass slides from citrate solutions. (a) Extinction spectra of samples A–G. (b–d) Transmission, reflectance, and absorption spectra, respectively, of samples A, E, and G.

showing intense extinctions up to ca. 550 nm. When the films are prepared on quartz, a series of five absorption bands are measured in the 200–500 nm spectral region (Figure S10 b, Supporting Information). The bands change in relative intensity and are red-shifted (except the band at 234 nm) when the morphology is changed from cubic to octahedral. Note that there is spectral correspondence between Cu_2O samples prepared on quartz and on glass substrates, but the relative intensity of the different bands may change between deposition batches.

Figure S10a (Supporting Information) presents photographs of glass slides coated with Cu_2O deposits. Paler films correspond to a smaller NC size, correlated with the total extinction in the UV–vis spectra (Figure 6a and Figure S10b, Supporting Information). The photographs demonstrate the good spatial homogeneity of the NC films over large areas achieved by means of the CD method.

Transmission and reflectance measurements (Figure 6b,c) enable calculation of the film absorption and evaluation of scattering effects. Scattering is relevant at wavelengths > 480 nm (Figure 6c), contributing to the high extinction in this spectral range. The reflectance trend is attributed to light scattering by increasingly large NCs, from sample G to A (Table 1). The calculated absorption spectra show characteristic bands at 450–480 nm (Figure 6d), which are not attributed to scattering.

Using the absorption spectra, the band-gap energy E_g of each NC film can be calculated using the Mott and Davis expression[77] (Figure S11, Supporting Information). The value obtained for sample G is E_g = 2.5 eV, decreasing to 2.3 eV for sample A (Cu_2O bulk value: 2.17 eV).

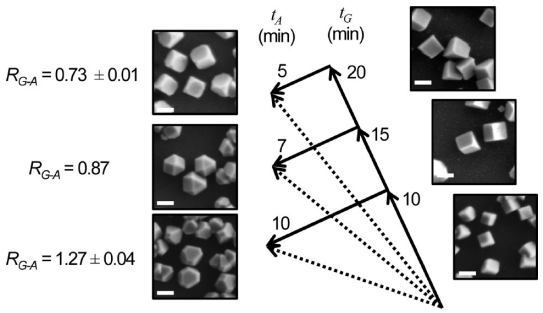

Figure 7. HRSEM images of Cu_2O NCs on glass substrates prepared by sequential deposition. Pregrown (in solution G) Cu_2O nanocubes of different sizes (controlled by the deposition time, t_G) are exposed to a solution promoting the octahedral morphology (solution A) for a time t_A. Vector lengths are proportional to the exposure times. Scale bars: 100 nm. Errors indicate standard deviations.

Sequential Depositions. Additional possibilities for controlling the Cu_2O NC morphology are provided by sequential deposition, *i.e.*, replacing the initial growth medium by a medium promoting a different crystal habit.

When cubic crystals pregrown in solution G are immersed in a solution promoting the octahedral habit (solution A), the initial cubic morphology is modified (Figure 7). The morphology and size of the final nanocrystals can be controlled by sequentially exposing the seeded substrate to solutions G and A for given times, t_G and t_A, respectively. The higher the ratio t_G/t_A, the more cubic-like are the final NCs.

In order to generate the entire range of possible cubic to octahedral morphologies, solutions A and G were chosen, as these solutions produce the highest and lowest R values, respectively, in one-step depositions.

Samples can be similarly prepared by reversing the order, namely, by pregrowing nanooctahedra in solution A followed by treatment in a solution promoting the cubic habit (solution G) (Figure S12, Supporting Information). However, when the order of exposure to the growth solutions is reversed, different t_G/t_A ratios are required for obtaining similar final morphologies. For instance, when starting with preformed octahedra, larger exposure times to solution G, compared to the exposure to solution A, are required in order to obtain similar cubic-like NCs. A different exposure order also affects the final NC surface density, as the use of a given initial solution defines the Cu_2O nucleation efficiency. Interestingly, secondary nucleation was not observed after changing the growth solution.

One can generally define R_{1-m}, *i.e.*, the R ratio for a sequence of m total deposition steps, as

$$R_{1-m} = \frac{\sum_{j=1}^{m} h_{<100>,j}}{\sum_{j=1}^{m} h_{<111>,j}} \quad (7)$$

where $h_{<hkl>,j}$ represent the variation in the distance from the *hkl* face to the Wulff point after the *j*th deposition period. For a two-step deposition, one can write

$$R_{1-2} = \frac{h_{<100>,1} + t_2 r_{<100>,2}}{h_{<111>,1} + t_2 r_{<111>,2}} \quad (8)$$

where $r_{<hkl>,2}$ is the growth rate in the $\langle hkl \rangle$ direction and t_2 is the deposition time for the second deposition step (for simplicity, growth rates are assumed to be constant). In the present work the growth solutions used are those promoting the extreme morphologies, *i.e.*, solutions A and G. Since the result of the first deposition step is either complete octahedra or complete cubes, the values of $r_{\langle 100 \rangle,1}$ and $r_{\langle 111 \rangle,1}$ cannot be simultaneously determined, which is the reason for the use of the experimental $h_{\langle 100 \rangle,1}$ and $h_{\langle 111 \rangle,1}$ for the first step in eq 8.

Equation 8 can be considered as the equivalent of $R = r_{\langle 100 \rangle}/r_{\langle 111 \rangle}$ used for a single deposition step, but with different initial conditions. Each type of crystal face grows at a different rate when using different solutions; that is, $r_{\langle 111 \rangle,1}$, $r_{\langle 100 \rangle,1}$, $r_{\langle 111 \rangle,2}$, and $r_{\langle 100 \rangle,2}$ are all different. The nonlinearity (in terms of deposition times) in sequential depositions is exhibited in eq 8, as R_{1-2} cannot be described by a simple linear combination of deposition times, but only by a complex function.

The case of sequential deposition with 10 min immersion time in each solution, producing tip-truncated octahedra ($R \approx 1.3$) irrespective of the treatment order (Figure 7 and Figure S12, Supporting Information), is an interesting coincidence, but not a general behavior. Reversing the order of exposure to the two growth solutions while maintaining the respective immersion times does not, as a rule, produce the same morphology (not shown).

Formation of tip-truncated octahedra when using equal deposition times in the different growth solutions implies that the growth rate of the {111} planes in solution A ($r_{\langle 111 \rangle,A}$) is higher than that of the {100} planes in solution G ($r_{\langle 100 \rangle,G}$), in agreement with the results of single-step CD (Figure 5).

Final R_{1-2} values in two-step depositions can be measured in a manner similar to that used in single-step depositions (measuring edge lengths) and interpreted according to eqs 7 and 8. The growth rates of the fast growing facets, $r_{\langle 100 \rangle,A}$ and $r_{\langle 111 \rangle,G}$, can then be estimated. To this end, $h_{\langle hkl \rangle,1}$ were substituted by the characteristic distances in cubic and octahedral NCs produced during the first step (which depend on the edge lengths, a_{tG} and c_{tA}, respectively), while $r_{\langle 111 \rangle,A}$ and $r_{\langle 100 \rangle,G}$ were replaced by their measured values from Figure 5, obtaining eqs 9 and 10 (see Supporting Information):

$$r_{\langle 100 \rangle,A} = \left(\frac{\sqrt{3}}{2}R_{G-A} - \frac{1}{2}\right)\frac{a_{tG}}{t_A} + R_{G-A} r_{\langle 111 \rangle,A} \quad (9)$$

$$r_{\langle 111 \rangle,G} = \left(\frac{1}{2R_{G-A}} - \frac{1}{\sqrt{6}}\right)\frac{c_{tA}}{t_G} + \frac{r_{\langle 100 \rangle,G}}{R_{A-G}} \quad (10)$$

The average values obtained are $r_{\langle 111 \rangle,G} = 5.3 \pm 1.4$ nm/min and $r_{\langle 100 \rangle,A} = 3.3 \pm 0.3$ nm/min, both higher than $r_{\langle 100 \rangle,G}$ and $r_{\langle 111 \rangle,A}$, as expected. These growth rates produce *R* values (for a single-step deposition) of 2.0 and 0.46 for solutions A and G, respectively, also in agreement with the expected *R* values of $R_A \geq 1.73$ and $R_G \leq 0.58$.

CONCLUSIONS

The physical properties and reactivity of Cu_2O NPs are determined by their crystalline morphology. In the present work precise morphology control was achieved using chemical (electroless) deposition of Cu_2O NCs on Au-seeded substrates in citrate-based solutions, covering the entire range of morphologies from complete cubes, *via* the intermediate morphologies truncated octahedra, cuboctahedra, and truncated cubes, to complete octahedra. The highly effective morphology control is attributed to competitive adsorption of hydroxide and citrate anions on the {100} and {111} planes of the growing crystallite. Sequential deposition using solutions promoting the two perfect morphologies provide additional possibilities of morphology design, while considering the relative NC growth rates.

Comparing the two solution-based methods for the deposition of Cu_2O NCs, *i.e.*, electrodeposition and CD, both may provide morphological control of the produced Cu_2O NCs under appropriate conditions. CD, however, is more general in terms of the choice of substrates. While electrodeposition is performed on conductive substrates serving as a cathode, we have carried out CD of Cu_2O NCs on a range of conducting, semiconducting, and insulating substrates, including glass, quartz, ITO, FTO, surface-oxidized carbon and polymeric supports, TiO_2, and others, obtaining similar results on all the substrates used.

The strategies presented here are generally applicable, enabling precise control over the crystalline morphology of Cu_2O NC films by CD on a wide range of substrates, suggesting a variety of possible applications.

EXPERIMENTAL SECTION

Materials. Hydrogen peroxide solution (30%, Frutarom), sulfuric acid (AR, 93–98%, Gadot), 3-(aminopropyl)trimethoxysilane (APTS) (97%, Aldrich), sodium tetrachloroaurate(III) (99.99%, Alfa Aesar), sodium borohydride (≥96%, Merck), paraformaldehyde powder (95%, Aldrich), copper(II) sulfate pentahydrate (>99.0%, Merck), sodium hydroxide pellets (>99.0%, Merck), trisodium citrate dihydrate (Na_3Cit) (>99.0%, Merck),

potassium sodium tartrate tetrahydrate (NaKT) (99.0%, Aldrich), (ethylenedinitrilo)tetraacetic acid disodium salt dihydrate ($Na_2H_2EDTA \cdot 2H_2O$) (99.0%, J. T. Baker), methanol (absolute, Biolab), and 2-propanol (>99.8%, Gadot) were used as received. Water was triply distilled. Samples were dried using N_2 flow obtained from a liquid N_2 household source.

Substrate Cleaning and Silanization. Microscope glass coverslides (Menzel-Gläser no. 3, 22 × 22 × 0.3 mm) and quartz slides (37 × 22 × 1 mm, Heraeus Quarzglas) were cut to 22 × 8 mm^2 and cleaned by immersion in freshly prepared hot "piranha" solution (1:3 H_2O_2/H_2SO_4) for >30 min (*Caution: piranha reacts violently with organic matter and should be handled with extreme care*), then thoroughly rinsed with triply distilled water and methanol. Cleaned slides were silanized by immersion in 1% v/v APTS in MeOH for 1 h, followed by thorough methanol and water rinsing.

Gold Seeding of Glass and Quartz Substrates. Gold seeds were formed by immersion of silanized (amine-terminated) slides in 5 mM aqueous $NaAuCl_4$ solution (pH = 2) for 2 min to electrostatically bind chloroaurate ions, rinsing with copious amounts of water, immersion in 50 mM aqueous $NaBH_4$ for 2 min to reduce the Au(III) ions to metallic Au clusters, rinsing thoroughly with water, and drying under a N_2 flow.

Chemical (Electroless) Deposition (CD). *Depositions from Citrate Solutions.* The following aqueous stock solutions were prepared: 1.5 M Na_3Cit (44.1% w/v) (S1); 0.64 M $CuSO_4 \cdot 5H_2O$ (16% w/v) (S2); 5 M NaOH (17.4% w/w) (S3); and 0.32 M formaldehyde, from hydrolyzed paraformaldehyde (S4). S1, S2, water, and S3 were added (see volumes in Scheme 2), in that order, into a 2 mL Eppendorf tube, which was closed and vortexed. S4 was then added, and the Eppendorf was vortexed again. An Au-seeded slide was placed in the closed tube, and CD of Cu_2O was allowed to proceed for 10 min, unless otherwise specified. The slide was then rinsed with water three times and dried under a N_2 stream. The deposition was carried out at room temperature (22−23 °C) under stationary conditions.

Depositions from EDTA Solutions. A 0.5 M Na_4EDTA solution was prepared by mixing $Na_2H_2EDTA \cdot 2H_2O$ (25.0 mmol, 9.306 g), NaOH (25.0 mmol, 1.00 g), and *ca.* 40 mL of H_2O. For achieving complete dissolution, a 5 M NaOH solution was added until the pH reached 8.15. The solution was then taken to volume in a 50 mL volumetric flask (S1′). EDTA-based Cu_2O CD solutions were prepared according to the procedure detailed above for Cu_2O CD from citrate solutions, replacing S1 with S1′. Unless otherwise specified, depositions were carried out for 20 min at room temperature (22−23 °C) under stationary conditions.

Depositions from Tartrate Solutions. A 1 M NaKT stock solution was prepared (S1″). NaKT-based Cu_2O CD solutions were prepared according to the procedure detailed above for Cu_2O CD from citrate solutions, replacing S1 with S1″. Depositions were carried out for 10 min at room temperature (22−23 °C) under stationary conditions.

Characterization Methods. *UV−Vis Spectroscopy.* Extinction spectra were obtained in the transmission mode using a Varian Cary 50 spectrophotometer operated at a wavelength resolution of 2 nm and an average acquisition time per point of 0.2 s. Combined transmission and total reflection measurements were carried out using a Jasco V570 UV/vis/NIR dual-beam spectrophotometer equipped with a model ISV-469 integration sphere, providing a spectral window in the range 400−850 nm. Baseline spectra were taken in air using Spectralon as the reflection standard.

Grazing Incidence X-ray Diffraction. Measurements were carried out at an incident angle of 2−3° using a TTRAX III powder diffractometer (Rigaku), equipped with a rotating Cu anode operating at 50 kV and 200 mA and with a multilayered mirror (CBO) forming a nearly parallel X-ray beam.

High-Resolution Scanning Electron Microscopy. HRSEM images were acquired with an ULTRA 55 FEG ZEISS HRSEM using the SE, in-lens and EsB detectors, at a voltage of 2 kV and a working distance of 3−4 mm. Slides were mounted on carbon tape loaded stubs and partially painted with carbon paste to increase the electrical conductivity and minimize charging. In some cases the sample conductivity was improved by sputtering 3 nm Cr on the slide (using an Emitech K575X sputter coater) before imaging. Analysis of HRSEM images was performed using the software ImageJ 1.42q (NIH, USA), measuring more than 100 particles per image.

Transmission Electron Microscopy (TEM). Nickel grids (SPI Supplies) supporting a nitrocellulose film onto which a thin carbon film was evaporated (Edwards) were surface oxidized in a UV-ozone cleaner (UVOCS T10×10/OES/E) for 5 min to provide surface carboxylation. APTS was then self-assembled on the grids in a 1% methanolic solution for 1 h, followed by rinsing with methanol (3×) and water. The grids were then Au seeded and coated with CD Cu_2O as described above, followed by iPrOH rinsing and drying. TEM measurements were carried out with a Philips CM-120 transmission electron microscope operating at 120 kV, equipped with a charge-coupled device camera (2k × 2k, Gatan Ultrascan 1000).

Conflict of Interest: The authors declare no competing financial interest.

Supporting Information Available: UV−vis spectra of solution A and variants thereof; particle size distributions in NCs; HRSEM showing odd-shaped $CuO/Cu(OH)_2$ prticles; evaluation of Cu_2O etching; tilted-angle HRSEM images; HRSEM images of NCs along different crystallographic directions; development of eqs 2 and 3; Cu_2O NC synthesis in EDTA and tartrate solutions; photographs and UV−vis spectra of slides A−G; band-gap energy calculations; HRSEM of Cu_2O NCs prepared by sequential deposition in reverse order. This material is available free of charge *via* the Internet at http://pubs.acs.org.

Acknowledgment. Support of this work by the Israel Science Foundation, grant no. 1251/11, and by the Grand Center for Sensors & Security (Weizmann Institute), is gratefully acknowledged. I.R. is Incumbent of the Agnes Spencer Professorial Chair of Physical Chemistry. The electron microscopy studies were conducted at the Irving and Cherna Moskowitz Center for Nano and Bio-Nano Imaging, Weizmann Institute of Science. This research is made possible in part by the historic generosity of the Harold Perlman family.

REFERENCES AND NOTES

1. Xia, Y.; Xiong, Y.; Lim, B.; Skrabalak, S. E. Shape-Controlled Synthesis of Metal Nanocrystals: Simple Chemistry Meets Complex Physics? *Angew Chem., Int. Ed.* **2009**, *48*, 60–103.
2. Pileni, M. P. Control of the Size and Shape of Inorganic Nanocrystals at Various Scales from Nano to Macrodomains. *J. Phys. Chem. C* **2007**, *111*, 9019–9038.
3. Liu, G.; Yu, J. C.; Lu, G. Q.; Cheng, H.-M. Crystal Facet Engineering of Semiconductor Photocatalysts: Motivations, Advances and Unique Properties. *Chem. Commun.* **2011**, *47*, 6763–6783.
4. Abdu, Y.; Musa, A. O. Copper (I) Oxide (Cu_2O) Based Solar Cells - A Review. *Bajopas* **2009**, *2*, 8–12.
5. Georgieva, V.; Tanusevski, A.; Georgieva, M., Low Cost Solar Cells Based on Cuprous Oxide. In *Solar Cells - Thin-Film Technologies*; Kosyachenko, L. A., Ed.; InTech, 2011.
6. Xiong, L.; Huang, S.; Yang, X.; Qiu, M.; Chen, Z.; Yu, Y. p-Type and n-type Cu_2O Semiconductor Thin Films: Controllable Preparation by Simple Solvothermal Method and Photoelectrochemical Properties. *Electrochim. Acta* **2011**, *56*, 2735–2739.
7. Hara, M.; Kondo, T.; Komoda, M.; Ikeda, S.; N. Kondo, J.; Domen, K.; Hara, M.; Shinohara, K.; Tanaka, A. Cu_2O as a Photocatalyst for Overall Water Splitting under Visible Light Irradiation. *Chem. Commun.* **1998**, 357–358.
8. Kuo, C. H.; Chen, C. H.; Huang, M. H. Seed-Mediated Synthesis of Monodispersed Cu_2O Nanocubes with Five Different Size Ranges from 40 to 420 nm. *Adv. Funct. Mater.* **2007**, *17*, 3773–3780.
9. Kuo, C.-H.; Huang, M. H. Facile Synthesis of Cu_2O Nanocrystals with Systematic Shape Evolution from Cubic to Octahedral Structures. *J. Phys. Chem. C* **2008**, *112*, 18355–18360.
10. Ho, J.-Y.; Huang, M. H. Synthesis of Submicrometer-Sized Cu_2O Crystals with Morphological Evolution from Cubic to

Hexapod Structures and Their Comparative Photocatalytic Activity. *J. Phys. Chem. C* **2009**, *113*, 14159–14164.
11. Xu, H.; Wang, W.; Zhu, W. Shape Evolution and Size-Controllable Synthesis of Cu_2O Octahedra and Their Morphology-Dependent Photocatalytic Properties. *J. Phys. Chem. B* **2006**, *110*, 13829–13834.
12. Zhang, J.; Liu, J.; Peng, Q.; Wang, X.; Li, Y. Nearly Monodisperse Cu_2O and CuO Nanospheres: Preparation and Applications for Sensitive Gas Sensors. *Chem. Mater.* **2006**, *18*, 867–871.
13. Shishiyanu, S. T.; Shishiyanu, T. S.; Lupan, O. I. Novel NO_2 Gas Sensor Based on Cuprous Oxide Thin Films. *Sensor. Actuat. B: Chem.* **2006**, *113*, 468–476.
14. Xu, Y.; Wang, H.; Yu, Y.; Tian, L.; Zhao, W.; Zhang, B. Cu_2O Nanocrystals: Surfactant-Free Room-Temperature Morphology-Modulated Synthesis and Shape-Dependent Heterogeneous Organic Catalytic Activities. *J. Phys. Chem. C* **2011**, *115*, 15288–15296.
15. White, B.; Yin, M.; Hall, A.; Le, D.; Stolbov, S.; Rahman, T.; Turro, N.; O'Brien, S. Complete CO Oxidation over Cu_2O Nanoparticles Supported on Silica Gel. *Nano Lett.* **2006**, *6*, 2095–2098.
16. Morales, J.; Sánchez, L.; Bijani, S.; Martínez, L.; Gabás, M.; Ramos-Barrado, J. R. Electrodeposition of Cu_2O: An Excellent Method for Obtaining Films of Controlled Morphology and Good Performance in Li-Ion Batteries. *Electrochem. Solid State* **2005**, *8*, A159–A162.
17. Dong, T. Y.; Wu, H. H.; Huang, C.; Song, J. M.; Chen, I. G.; Kao, T. H. Octanethiolated Cu and Cu_2O Nanoparticles as Ink to Form Metallic Copper Film. *Appl. Surf. Sci.* **2009**, *255*, 3891–3896.
18. Lee, Y.-J.; Kim, S.; Park, S.-H.; Park, H.; Huh, Y.-D. Morphology-Dependent Antibacterial Activities of Cu_2O. *Mater. Lett.* **2010**, *65*, 818–820.
19. Ristov, M.; Sinadinovski, G.; Grozdanov, I. Chemical Deposition of Cu_2O Thin Films. *Thin Solid Films* **1985**, *123*, 63–67.
20. Grozdanov, I. Electroless Chemical Deposition Technique for Cu_2O Thin Films. *Mater. Lett.* **1994**, *19*, 281–285.
21. Greenberg, C. B.; Breininger, J. S. Electroless Deposition of Cuprous Oxide. *J. Electrochem. Soc.* **1977**, *124*, 1681–1685.
22. Sharma, R.; Hahn, Y.-B. Nanocrystalline Thin Films of Cu, CuO and Cu_2O Synthesized by Electroless Deposition. *Sci. Adv. Mater.* **2012**, *4*, 23–28.
23. Zhao, X.; Bao, Z.; Sun, C.; Xue, D. Polymorphology Formation of Cu_2O: A Microscopic Understanding of Single Crystal Growth from Both Thermodynamic and Kinetic Models. *J. Cryst. Growth* **2009**, *311*, 711–715.
24. Susman, M. D.; Feldman, Y.; Vaskevich, A.; Rubinstein, I. Chemical Deposition and Stabilization of Plasmonic Copper Nanoparticle Films on Transparent Substrates. *Chem. Mater.* **2012**, *24*, 2501–2508.
25. Norkus, E.; Kepenienė, V.; Vaškelis, A.; Jačiauskienė, J.; Stalnionienė, I.; Stalnionis, G.; Macalady, D. L. Application of Environmentally Friendly Ligands for Alkaline Electroless Copper Plating Systems: Electroless Copper Deposition Using Trisodium Salt of 2-Hydroxy-1,2,3-propanetricarboxylic Acid as Cu(II) Ligand. *Chemija* **2006**, *17*, 20–29.
26. Zhang, D.-F.; Zhang, H.; Guo, L.; Zheng, K.; Han, X.-D.; Zhang, Z. Delicate Control of Crystallographic Facet-Oriented Cu_2O Nanocrystals and the Correlated Adsorption Ability. *J. Mater. Chem.* **2009**, *19*, 5220–5225.
27. Siegfried, M. J.; Choi, K.-S. Directing the Architecture of Cuprous Oxide Crystals during Electrochemical Growth. *Angew. Chem., Int. Ed.* **2005**, *44*, 3218–3223.
28. Siegfried, M. J.; Choi, K.-S. Elucidating the Effect of Additives on the Growth and Stability of Cu_2O Surfaces *via* Shape Transformation of Pre-Grown Crystals. *J. Am. Chem. Soc.* **2006**, *128*, 10356–10357.
29. Siegfried, M. J.; Choi, K. S. Electrochemical Crystallization of Cuprous Oxide with Systematic Shape Evolution. *Adv. Mater.* **2004**, *16*, 1743–1746.
30. Wang, Z.; Wang, H.; Wang, L.; Pan, L. Controlled Synthesis of Cu_2O Cubic and Octahedral Nano- and Microcrystals. *Cryst. Res. Technol.* **2009**, *44*, 624–628.
31. Wang, W.; Liao, Z.; Wang, Y.; Wu, X.; Qu, F.; Zhang, X. Hydrothermal Synthesis of Highly Symmetric 26-Facet Cu_2O Polyhedra. *Cryst. Res. Technol.* **2011**, *46*, 300–304.
32. Lan, X.; Zhang, J.; Gao, H.; Wang, T. Morphology-Controlled Hydrothermal Synthesis and Growth Mechanism of Microcrystal Cu_2O. *CrystEngComm* **2011**, *13*, 633–636.
33. Kim, M. H.; Lim, B.; Lee, E. P.; Xia, Y. Polyol Synthesis of Cu_2O Nanoparticles: Use of Chloride to Promote the Formation of a Cubic Morphology. *J. Mater. Chem.* **2008**, *18*, 4069–4073.
34. Xu, L.; Jiang, L.-P.; Zhu, J.-J. Sonochemical Synthesis and Photocatalysis of Porous Cu_2O Nanospheres with Controllable Structures. *Nanotechnology* **2009**, *20*, 045605.
35. Gou, L.; Murphy, C. J. Solution-Phase Synthesis of Cu_2O Nanocubes. *Nano Lett.* **2003**, *3*, 231–234.
36. Gou, L.; Murphy, C. J. Controlling the Size of Cu_2O Nanocubes from 200 to 25 nm. *J. Mater. Chem.* **2004**, *14*, 735–738.
37. Tang, A.; Xiao, Y.; Ouyang, J.; Nie, S. Preparation, Photo-Catalytic Activity of Cuprous Oxide Nano-Crystallites with Different Sizes. *J. Alloys Compd* **2008**, *457*, 447–451.
38. Yang, Z.; Sun, S.; Kong, C.; Song, X.; Ding, B. Designated-Tailoring on {100} Facets of Cu_2O Nanostructures: From Octahedral to Its Different Truncated Forms. *J. Nanomater.* **2010**, 2010.
39. Sui, Y.; Fu, W.; Yang, H.; Zeng, Y.; Zhang, Y.; Zhao, Q.; Li, Y.; Zhou, X.; Leng, Y.; Li, M.; Zou, G. Low Temperature Synthesis of Cu_2O Crystals: Shape Evolution and Growth Mechanism. *Cryst. Growth Des.* **2009**, *10*, 99–108.
40. Sun, S.; Song, X.; Sun, Y.; Deng, D.; Yang, Z. The Crystal-Facet-Dependent Effect of Polyhedral Cu_2O Microcrystals on Photocatalytic Activity. *Catal. Sci. Technol.* **2012**, *2*, 925–930.
41. Wang, Y.-j.; Zhou, K.-g. Effect of OH^- on Morphology of Cu_2O Particles Prepared through Reduction of Cu(II) by Glucose. *J. Cent. South Univ.* **2012**, *19*, 2125–2129.
42. Guo, S.; Fang, Y.; Dong, S.; Wang, E. Templateless, Surfactantless, Electrochemical Route to a Cuprous Oxide Microcrystal: From Octahedra to Monodisperse Colloid Spheres. *Inorg. Chem.* **2007**, *46*, 9537–9539.
43. Radi, A.; Pradhan, D.; Sohn, Y.; Leung, K. T. Nanoscale Shape and Size Control of Cubic, Cuboctahedral, and Octahedral Cu-Cu_2O Core-Shell Nanoparticles on Si(100) by One-Step, Templateless, Capping-Agent-Free Electrodeposition. *ACS Nano* **2010**, *4*, 1553–1560.
44. Rakhshani, A. E.; Al-Jassar, A. A.; Varghese, J. Electrodeposition and Characterization of Cuprous Oxide. *Thin Solid Films* **1987**, *148*, 191–201.
45. Rakhshani, A. E.; Varghese, J. Galvanostatic Deposition of Thin Films of Cuprous Oxide. *Sol. Energ. Mater.* **1987**, *15*, 237–248.
46. Rakhshani, A. E.; Varghese, J. Potentiostatic Electrodeposition of Cuprous Oxide. *Thin Solid Films* **1988**, *157*, 87–96.
47. Golden, T. D.; Shumsky, M. G.; Zhou, Y.; VanderWerf, R. A.; Van Leeuwen, R. A.; Switzer, J. A. Electrochemical Deposition of Copper(I) Oxide Films. *Chem. Mater.* **1996**, *8*, 2499–2504.
48. Zhou, Y.; Switzer, J. A. Electrochemical Deposition and Microstructure of Copper (I) Oxide Films. *Scr. Mater.* **1998**, *38*, 1731–1738.
49. Balamurugan, B.; Mehta, B. R. Optical and Structural Properties of Nanocrystalline Copper Oxide Thin Films Prepared by Activated Reactive Evaporation. *Thin Solid Films* **2001**, *396*, 90–96.
50. Chen, A.; Long, H.; Li, X.; Li, Y.; Yang, G.; Lu, P. Controlled Growth and Characteristics of Single-Phase Cu_2O and CuO Films by Pulsed Laser Deposition. *Vacuum* **2009**, *83*, 927–930.
51. Al-Kuhaili, M. F. Characterization of Copper Oxide Thin Films Deposited by the Thermal Evaporation of Cuprous Oxide (Cu_2O). *Vacuum* **2008**, *82*, 623–629.
52. Jayatissa, A. H.; Guo, K.; Jayasuriya, A. C. Fabrication of Cuprous and Cupric Oxide Thin Films by Heat Treatment. *Appl. Surf. Sci.* **2009**, *255*, 9474–9479.

53. Akimoto, K.; Ishizuka, S.; Yanagita, M.; Nawa, Y.; Paul, G. K.; Sakurai, T. Thin Film Deposition of Cu_2O and Application for Solar Cells. *Sol. Energy* **2006**, *80*, 715–722.
54. Yu, Z. Q.; Wang, C. M.; Engelhard, M. H.; Nachimuthu, P.; McCready, D. E.; Lyubinetsky, I. V.; Thevuthasan, S. Epitaxial Growth and Microstructure of Cu_2O Nanoparticle/Thin Films on $SrTiO_3$(100). *Nanotechnology* **2007**, *18*, 115601.
55. Machefert, J. M.; D'Huysser, A.; Lenglet, M.; Lopitaux, J.; Delahaye, D. Initial Stage of Copper Thermal Oxidation Studied by UV-Vis-NIR Reflectance Spectroscopy, XPS and X-ray Diffraction. *Mater. Res. Bul* **1988**, *23*, 1379–1388.
56. Derin, H.; Kantarli, K. Optical Characterization of Thin Thermal Oxide Films on Copper by Ellipsometry. *Appl. Phys. A: Mater* **2002**, *75*, 391–395.
57. Rakhshani, A. E. Preparation, Characterization and Photovoltaic Properties of Cuprous Oxide - A Review. *Solid-State Electron.* **1986**, *29*, 7–17.
58. Ray, S. C. Preparation of Copper Oxide Thin Film by the Sol-Gel-like Dip Technique and Study of Their Structural and Optical Properties. *Sol. Energy Mater. Sol. Cells* **2001**, *68*, 307–312.
59. Susman, M. D.; Vaskevich, A.; Rubinstein, I. Unpublished results.
60. Zhang, W.; Chen, Z.; Yang, Z. An Inward Replacement/Etching Route to Synthesize Double-Walled Cu_7S_4 Nanoboxes and Their Enhanced Performances in Ammonia Gas Sensing. *Phys. Chem. Chem. Phys.* **2009**, *11*, 6263–6268.
61. Ng, K. H.; Penner, R. M. Electrodeposition of Silver-Copper Bimetallic Particles Having Two Archetypes by Facilitated Nucleation. *J. Electroanal. Chem.* **2002**, *522*, 86–94.
62. Norkus, E.; Kepenienė, V.; Vaškelis, A.; Jačiauskienė, J.; Stalnionienė, I.; Stalnionis, G. Application of Environmentally Friendly Ligands for Alkaline Electroless Copper Plating Systems: Electroless Copper Deposition Using Trisodium Salt of 2-Hydroxy-1,2,3-propanetricarboxylic Acid as Cu(II) Ligand. *Chemija* **2006**, *17*, 20–29.
63. Schoenberg, L. N. The Structure of the Complexed Copper Species in Electroless Copper Plating Solutions. *J. Electrochem. Soc.* **1971**, *118*, 1571–1576.
64. Murray, C. N.; Riley, J. P. The Solubility of Gases in Distilled Water and Sea Water - II. Oxygen. *Deep-Sea Res. Part I* **1969**, *16*, 311–320.
65. Kuo, C.-H.; Hua, T.-E.; Huang, M. H. Au Nanocrystal-Directed Growth of Au-Cu_2O Core-Shell Heterostructures with Precise Morphological Control. *J. Am. Chem. Soc.* **2009**, *131*, 17871–17878.
66. Dhanaraj, G.; Byrappa, K.; Prasad, V.; Dudley, M. *Springer Handbook of Crystal Growth*; Springer: Berlin, 2010.
67. Kaishew, R. Equilibrium Shape and Nucleation Work of Crystals on Substrates. *Commun. Bulg. Acad. Sci.* **1950**, *1*, 100–139.
68. Budevski, E. B.; Staikov, G. T.; Lorenz, W. J. *Electrochemical Phase Formation and Growth: An Introduction to the Initial Stages of Metal Deposition*; John Wiley & Sons: New York, 2008.
69. Winterbottom, W. L. Equilibrium Shape of a Small Particle in Contact with a Foreign Substrate. *Acta Metall. Mater.* **1967**, *15*, 303–310.
70. Bühler, J.; Prior, Y. Study of Morphological Behavior of Single Diamond Crystals. *J. Cryst. Growth* **2000**, *209*, 779–788.
71. Wild, C.; Koidl, P.; Müller-Sebert, W.; Walcher, H.; Kohl, R.; Herres, N.; Locher, R.; Samlenski, R.; Brenn, R. Chemical Vapour Deposition and Characterization of Smooth {100}-Faceted Diamond Films. *Diam. Relat. Mater.* **1993**, *2*, 158–168.
72. Clausing, R. E.; Heatherly, L.; Horton, L. L.; Specht, E. D.; Begun, G. M.; Wang, Z. L. Textures and Morphologies of Chemical Vapor Deposited (CVD) Diamond. *Diam. Relat. Mater.* **1992**, *1*, 411–415.
73. Wang, D.; Mo, M.; Yu, D.; Xu, L.; Li, F.; Qian, Y. Large-Scale Growth and Shape Evolution of Cu_2O Cubes. *Cryst. Growth Des.* **2003**, *3*, 717–720.
74. Schulz, K. H.; Cox, D. F. Photoemission and Low-Energy-Electron-Diffraction Study of Clean and Oxygen-Dosed Cu_2O (111) and (100) Surfaces. *Phys. Rev. B* **1991**, *43*, 1610–1621.
75. Bindra, P.; White, J. R. Fundamental Aspects of Electroless Copper Plating. In *Electroless Plating - Fundamentals and Applications*; Mallory, G. O.; Hajdu, J. B., Eds.; American Electroplaters and Surface Finishers Society: Orlando, Florida, USA, 1990; pp 289−329.
76. Banerjee, S.; Chakravorty, D. Optical Absorption by Nanoparticles of Cu_2O. *Europhys. Lett.* **2000**, *52*, 468–473.
77. Mott, N. F.; Davis, E. A., *Electronic Processes in Non-Crystalline Materials*; Clarendon Press: Oxford, 1979.